Carbon Dioxide "Trapped" in a β–Carbonic Anhydrase

Mayank Aggarwal[1], Teck Khiang Chua[2], Melissa A. Pinard[3], Doletha M. Szebenyi[2], and Robert McKenna[3*]

[1]Division of Biology and Soft Matter, Oak Ridge National Laboratory, Oak Ridge, TN 37831.

[2]Cornell High Energy Synchrotron Source (CHESS), Cornell University, Ithaca, NY 14853.

[3]Department of Biochemistry and Molecular Biology, College of Medicine, University of Florida, Gainesville, FL 32610.

[*]Corresponding author:

Phone: (352) 392-5696

Email: rmckenna@ufl.edu

Keywords: β-carbonic anhydrase, *Pseudomonas aeruginosa*, CO_2 binding.

Abbreviations: CA (Carbonic Anhydrase), ZBS (Zinc Bound Solvent), PDB (Protein Data Bank), RMSD (Root Mean Square Deviation).

Abstract

Carbonic anhydrases (CAs) are enzymes that catalyze the hydration/dehydration of CO_2/HCO_3^- with rates approaching diffusion controlled limits ($k_{cat}/K_M \sim 10^8$ $M^{-1}s^{-1}$). This family of enzymes has evolved disparate protein folds that all perform the same reaction at near catalytic perfection. Presented here is a structural study of a beta-CA (psCA3) expressed in *Pseudomonas aeruginosa*, in complex with CO_2, using pressurized cryo-cooled crystallography. The structure has been refined to 1.6 Å resolution with an R_{cryst}/R_{free} of 17.3/19.9 % and is compared with the alpha-CA, human CA isoform II (hCA II), the only other CA to have CO_2 captured in its active site. Despite no structural similarity between psCA3 and hCA II, the CO_2 binding orientation relative to the zinc-bound solvent is identical. In addition, a second CO_2 binding site was located at the dimer interface of psCA3. Interestingly, all beta-CAs function as dimers or higher order oligomeric states, and the CO_2 bound at the interface may contribute to the allosteric nature of this family of enzymes and/or act as a CO_2 sensor, forming the dimer only at a CO_2 concentration threshold level, to form the active site.

Carbonic anhydrases (CAs; EC 4.2.1.1) are metalloenzymes that catalyze the reversible interconversion of CO_2 and HCO_3^-. All CAs follow a two-step ping pong mechanism. In the hydration direction, CO_2 enters the active site where it undergoes nucleophilic attack by a metal-bound hydroxide (the metal is a zinc ion, in most cases), is converted into HCO_3^-, and then displaced by a water molecule. In the second step of the reaction, the metal-bound water transfers a proton to the bulk solvent to regenerate the metal-bound hydroxide in readiness for the next cycle of catalysis [1,2].

CAs are ubiquitous and found in the deepest branches of life. Demonstrating evolutionary convergence, currently five CA classes have been identified, termed α, β, γ, δ and ζ, with little to no structural homology. To date all α- and β-CAs have been shown to be zinc metalloenzymes. The α-CAs have been the most extensively studied because of their role in human pathology and drug targeting; however, the other classes play a greater role in the global carbon cycle [1]. In plants, β-CAs are required for transport and maintenance of CO_2 and HCO_3^- concentrations for photosynthesis, and similarly in prokaryotes they are involved in the maintenance of internal pH and CO_2/HCO_3^- concentrations required for biosynthetic reactions. Unlike the α-CAs, the β-CAs exhibit a much greater phylogenetic diversity [3,4]. Their importance in prokaryotic biology can be deduced from their widespread presence in metabolically diverse species [4]. The β-CAs play an essential role in facilitating aerobic growth of microbes at low partial pressures of CO_2 by providing endogenous HCO_3^- [5–10]. Additionally, β-CAs are involved in multiple roles such as cyanate degradation, host colonization, host survival, and growth in different organisms [11–13]. Although -βCAs are essential for growth of microbes such as *Escherichia coli* [8], *Corynebacterium glutamicum* [9], *Saccharomyces cerevisiae* [14], and *Helicobacter pylori* [15], their full physiological role in the biosphere is still to be discovered [16].

Pseudomonas aeruginosa (P. aeruginosa) is a widely distributed environmental pathogenic bacterium that can cause diseases in animals, including humans. Especially in immune-compromised or otherwise susceptible hosts (patients with HIV, cancer, or burns), it can cause a severe infection of the heart, urinary tract, lungs, and wounds [17,18]. It is also one of the major pathogenic bacteria that cause nosocomial infections [19]. *P. aeruginosa* is found in a wide variety of habitats, so it has evolved a mechanism to thrive in environments with different concentrations of CO_2. This adaptation is particularly helpful for the bacteria when infecting lungs, which have ~200 times higher concentration of CO_2 as compared to atmospheric levels (400 ppm) [20]; the solubility of CO_2 in water at 298 K is 55 mM [21]. Since *P. aeruginosa* is resistant to most available antibiotics [19], β-CAs also offer a new target for antibiotic development. Lotlikar *et al.* have identified three genes coding for three β-CAs (psCA1-3) in *P. aeruginosa* PAO1 [22].

Most CAs are extremely fast enzymes that function at a rate that approaches the diffusion controlled limit ($k_{cat}/K_M \sim 10^8$ $M^{-1}s^{-1}$) and follow Michaelis-Menten kinetics. The overall fold and oligomeric state of the α- and β-CAs are very different. The α-CAs are mainly monomers (there are a few reported cases of dimers, e.g. hCAs IX and XII, but both of these can function as monomers) with an extended 10 stranded twisted β-sheet, flanked by 6 or more α-helices [2,23]. In contrast, the β-CAs are only functional as dimers or larger oligomeric states and have more compact structures: a β-sheet core composed of 4 or 5 strands, and 4 or more α-helices surrounding this core. Interestingly, the active sites of α- and β-CAs do exhibit certain architectural similarities. In both classes, the active sites are clearly divided into two regions – hydrophobic and hydrophilic (Figure 1A and 1B). In the α-CAs, the active site zinc is located at the base of a 15 Å deep conical cleft, coordinated by three histidines, and highly solvated (20

ordered waters in human (h) CA II), whereas the β-CAs have a much shallower (<10 Å) active site, constructed by the dimer formation; in an active configuration the zinc is coordinated by two cysteines and a histidine, and sparsely solvated (4 ordered waters in psCA3) (Figure 1C and 1D). This implies that the mechanism of proton transfer is most likely different between the two CA classes. In α-CAs, this function is carried out by a well ordered network of water molecules and a histidine proton shuttle residue (His64 in hCAII) (Figure 1C) [24]. In contrast, site directed mutagenesis on β-CAs, has led to the widely accepted view that a combination of residues are responsible for proton shuttling, and the identity of the residues differs among β-CAs [25–27]. However, a unique arrangement of partially conserved amino acid residues in the active site (Arg-Asp dyad, for example) is thought to play an important role in a pH induced catalytic switch in the opening and closing of the active site, by displacing a zinc-bound solvent molecule (ZBS) (Figure 1D). The ZBS, which can be either OH^- or H_2O (depending on the pH of the system) [16], is the fourth ligand of the tetrahedrally coordinated zinc for both α- and β-CAs in an active state.

As the CO_2 substrate has no dipole moment, it is expected to bind weakly in the active site of these enzymes [28]. The dissociation constant of CO_2 measured for hCA II has been calculated to be 100 mM. This makes capture of the substrate technically difficult; in fact, until this study only hCA II has been determined in complex with CO_2, using CO_2-pressurized cryo-cooled crystallography [28,29].

Here we present the first structure of CO_2 bound to a β-CA, psCA3, which has allowed a comparison of CO_2 binding in two structurally disparate CAs that have undergone convergent evolution to perform the same enzymatic reaction.

Experimental Procedures

Expression, Purification, and Crystallization of psCA3

Cloning, expression and purification were carried out as described previously [22]. The recombinant gene PA4676 was expressed in *E. coli* BL21 (DE3) cells with a His-tag. The culture was grown at 37 ºC in the presence of ampicillin (100 μg/mL) until it reached an OD_{600} of 1.0, and thereafter induced overnight with isopropyl β-D-1-thiogalactopyranoside (IPTG) (100 μg/mL) for protein expression. Cells were re-suspended in lysis buffer (20 mM Tris, 5 mM imidazole, 150 mM NaCl, pH 7.9) and lysed by sonication. Protein lysate was collected after centrifuging the lysed cells at 16,000 rpm for 50 minutes, and purified using His-tag column chromatography using a Sepharose column. Non-specifically bound proteins were washed off the column using lysis buffer, and wash buffer (lysis buffer with 60 mM imidazole); finally, the protein was eluted with elution buffer (lysis buffer with 300 mM imidazole). The eluted protein was then dialyzed (in 20 mM Tris, pH 8.3) to remove imidazole, and thereafter concentrated to 10 mg/mL using a 10 kDa filter. The crystallization condition of psCA3 crystals was optimized using the hanging-drop vapor diffusion technique. 500 μL reservoir solution containing 50% polyethylene glycol 200, 0.1 M Tris-HCl at pH 7.0 was placed in vapor equilibration with a drop size of 5 μL reservoir solution and 5 μL psCA3 protein. The psCA3 crystals were crystallized after six days and grew to approximate dimensions of 400 × 150 × 150 μm.

CO_2 Binding

In order to capture CO_2 in the crystals of psCA3, CO_2 was used as a pressurizing agent during the cryo-cooling process as described below. Using the capillary shielding method [30],

psCA3 crystals were picked and soaked into 20 mM Tris-HCl pH 7, 10% PEG 200, and 10% glycerol cryoprotectant solution and inserted into one end of a capillary tube (inside diameter = 991 μm, wall = 25.4 μm; Advanced Polymers, Salem, NH, USA) to prevent crystal dehydration. The other end of the capillary tube was then filled with 4 μL cryoprotectant to form a reservoir without touching the crystal. The cryoloop assembly was loaded into a high-pressure tube [31], where the crystals were pressurized with 9 bars of CO_2 for 10 min. Without releasing the CO_2 pressure, the crystals were slowly frozen over 2 min by dipping the sealed end of the pressure tubes into liquid nitrogen. During this time the gas pressure was observed to drop below 1 bar as the CO_2 solidified [28]. The cooled crystals were then recovered from the high-pressure tubes in liquid nitrogen and transferred into a dewar for storage before data collection [31].

X-ray Data Collection and Processing

A total of 360 X-ray diffraction image frames were collected at Cornell High Energy Synchrotron Source (CHESS, New York), beamline F1, at a wavelength of 0.978 Å. Data were collected using the oscillation method in intervals of 1^o on an ADSC Quantum 210 CCD detector (Area Detector Systems Corp.), with a crystal to detector distance of 195 mm. X-ray diffraction data indexing, integration, and scaling were performed using *HKL2000* [32]. The data were scaled to a resolution of 1.6 Å, with an overall completeness and R_{sym} of 99.3% and 8.0%, respectively (Table 1).

Molecular Replacement and Structure Determination

Starting phases were calculated using molecular replacement from PDB ID: 4RXY [33], with waters removed. The PHENIX package [34] was used for refinement. Randomly selected 5% of the unique reflections were excluded from the refinement data set for the purpose of R_{free} calculations[35], and refinements were alternated with manual refitting of the model in *COOT* [36].

Results

The protein psCA3 crystallized in space group *I*222, with unit cell dimensions 71.8, 78.1, and 87.7 Å. The data were phased using coordinates from the recently determined psCA3 structure (PDB ID: 4RXY [33]). The crystallographic asymmetric unit contains a psCA3 dimer. The structure was refined to a resolution of 1.6 Å, with an R_{cryst}/R_{free} of 0.17/0.19; the first two residues were disordered. The crystallographic data collection and refinement statistics are given in Table 1 and the coordinates and structure factors have been deposited in the protein data bank with PDB ID: 5BQ1. After initial refinement of the structure, a difference (F_o-F_c) map clearly showed electron density corresponding to three CO_2 binding locations in the psCA3 dimer. As expected, two were positioned in each active site, while the third appeared unexpectedly at the dimeric interface, sandwiched between the two monomers (Figure 2).

Active Site CO_2 Binding Site

CO_2 was observed bound in the active site of each of the psCA3 monomers. As seen in the case of hCA II, the CO_2 displaced a water, termed "deep water" that in the unbound state lies in the hydrophobic pocket and is stabilized by a short strong hydrogen bond (~ 2.6 Å) with the

ZBS [28] (Figure 3A). The CO_2 resides within the hydrophobic cleft formed by Val66, Gly102, Gly103, and Phe61', Phe83', Val87', and Leu88' (from the second monomer). The CO_2 proximal oxygen is 2.8 Å from the ZBS, with an O-ZBS-Zn angle of 113°, thereby orienting the CO_2 towards the zinc. In addition, the CO_2 is further stabilized by H-bonds with the side-chain oxygen of Gln33' from the adjacent monomer (3.4 Å), and the backbone amide N of Gly103 (3.3 Å) (Figure 3B).

Dimer Interface CO_2 Binding Site

Unexpectedly, a third bound CO_2 was observed buried in the dimer interface, sandwiched between the symmetry paired residues Ala49, Val62, and Arg64. The oxygens of CO_2 are stabilized by two paired H-bonds with the side chains of Arg64 (from each monomer), with additional stabilization by the hydrophobic residues of Ala49 and Val62 (Figure 4). Based only on structural observations, the dimer interface CO_2 would appear more stable than the active site CO_2, as it is completely buried with more stabilizing interactions (in terms of hydrogen bonds and buried surface area) and has a refined B-factor of 22.4 compared to 40.6 $Å^2$ for the active site bound CO_2 (Table 1).

Overall Structure

Superposition of the psCA3 structures in unbound state (PDB ID: 4RXY[33]) onto the complex with CO_2 (reported here) showed a main chain r.m.s.d. of ~0.3 Å, implying very little structural movement on substrate binding. However, slight structural perturbations in the side

chains of Val66 and Phe81' in the active site were observed. Val66 moved ~0.5 Å away from the catalytic zinc, possibly due to repulsion from the electronegative oxygens of CO_2, and Phe81' moved ~0.7 Å towards the active site, due to attractive hydrophobic and van der Waals forces on the carbon atom in CO_2 (Figure 6).

Discussion

This work describes the first structure of a β-CA in complex with its substrate CO_2, generated by pressurizing a crystal of psCA3 at room temperature with > 5 atm CO_2, and flash cooling it in liquid nitrogen, as described previously by our group for the α-CA, hCA II[28]. The reason this method is able to capture the substrate without catalysis is that as the crystal is exposed to CO_2, the pH is reduced to below 6.0 and the ZBS (which would be OH^- for the catalysis to occur in the hydration direction) gains a proton and becomes a water molecule. As a result of this, CA can no longer carry out the CO_2 to HCO_3^- forward reaction. Thus, the CO_2 is stably bound in the active site (Figures 2 and 3).

At first, this seems like a reasonable and simple explanation for the observed CO_2 binding, and is the argument used when CO_2 was first capture in hCA II[28]. But the β-CAs class is further divided into two types, based on the structural organization of their active site configuration and catalytic pH range. Type I is active over a broad pH range, while type II is active only for an alkaline pH range. With type I, the zinc is coordinated by three residues and the ZBS (an open active site, over a large pH range, Figure 1D); whereas in type II, the zinc is in an open state at an alkaline pH, but coordinated by four residues (Asp from the Asp-Arg dyad, in a closed state), at low pH[37,38].

The type II βCAs have been shown to "switch" from an active (R) to an inactive (T) state at lower pH[18]. Interestingly, the β-CA psCA3 used in this study has been previously shown to be a type II; hence, at the pH of this study the Asp-Arg dyad should have switched conformation to the closed state and displaced the ZBS, thereby eliminating the CO_2 binding site[22]. However, in unpublished studies we soaked crystals of psCA3 (initially grown at pH 7) in solutions with pH < 6, and they never underwent the pH induced structural switch. Therefore, it can be argued that crystal packing constraints of psCA3 may inhibit this conformational switch; in another packing configuration the Asp-Arg dyad might be induced to transform to the T state. These studies are now ongoing. A direct H-bond between CO_2 and Gln33' is particularly interesting as it supports the previously reported and hypothesized importance of Gln33' (or its equivalent in β-CAs from other organisms) in stabilization of the transition state during the conversion of CO_2 to HCO_3^-. This finding is a direct corroboration of the proposed role of Gln33' as suggested by site directed mutagenesis[39].

Despite being disparate and evolutionarily distinct structures, the CO_2 active binding sites for psCA3 and hCA II are remarkably similar. In both, the CO_2 is located in a hydrophobic pocket defined by five residues: in psCA3 the residues are Phe61' Val66', Phe83', Val87', and Leu88', while in hCA II they are Val121, Val135, Leu141, Val143, and Trp209, with some differences in amino acid type and spatial arrangement. Both have an aromatic amino acid (Phe83' in psCA3 and Trp209 in hCA II) as the assembly core of the hydrophobic cluster cavity. In addition, even though the active site of psCA3 is much shallower and has fewer waters than hCA II, it is noteworthy that the CO_2 buries 129.7 $Å^2$ (~87% of its total surface area), comparable to that in hCA II (128.1 $Å^2$). These surface area calculations were performed using PDBePISA[40] (Figure 5). Also, relative to the zinc the orientation of the CO_2 is almost identical,

with the CO_2 central carbon aligned and distanced 2.8 Å from the ZBS, presumably in readiness for nucleophilic attack. The ZBS is stabilized by a H-bond with Thr199 in HCA II and Asp44 in psCA3 (Figure 5).

Unexpected was the discovery of an additional CO_2 binding site at the dimer interface of psCA3, where the CO_2 is completely surface "inaccessible" and stabilized by four H-bonds. Of course, in the case of hCA II, which functions as a monomer, this interface does not exist. Hence, this dimer binding site begs the question, "how does the CO_2 bind and does it have implications for enzyme function, as the active site only forms when psCA3 is a dimer (Figures 1B & 1D)?"

It is known that β-CAs, unlike α-CAs, exhibit allostery[16]. Studies have shown the existence of a non-catalytic bicarbonate ion binding site in *Haemophilus influenza* β-CA (HICA, PDB ID: 2A8D[38]) and *Escherichia coli* β-CA (ECCA, PDB ID: 1I6P[41]) that is characterized by a Trp39-Arg64-Tyr181 (HICA numbering) triad. In these type II β-CAs, binding of a bicarbonate ion in this allosteric site relocates the side chain of Val47 (HICA numbering) and causes the reorganization of the 44-48 loop; the Asp44-Arg46 dyad is also disrupted. Interestingly, psCA3 also contains this Trp39-Arg64-Tyr182 triad (psCA3 numbering). Though bicarbonate was not found bound in this potential allosteric binding site, the CO_2 molecule at the dimer interface was ~6 Å from this site. The CO_2 at this site is completely buried and the only way this molecule could have entered this site seems to be due to the protein dynamics and molecular "breathing". Possibly, under alkaline pH conditions, CO_2 would be converted into HCO_3^- and bind in the allosteric site; it might then adopt the closed active site configuration as its loop 44-48 underwent reorganization. In addition to HCO_3^-, other ions such as sulfate[38], phosphate[39], and chloride[42] and ions have also been earlier reported to be bound at this site. Hence, we suggest that though this site may have a biochemical, structural, and physiological role to play and is not just an

experimental artefact caused by exposure to pressurized $CO_{2,}$ it could also just be a highly promiscuous site that can potentially bind many different small molecules.

Funding Information

This work has been funded by Shull Fellowship awarded to MA at ORNL, and NIH grant GM25154.

Acknowledgement

The authors would also like to thank the staff at CHESS and MacCHESS, Cornell University, NY for their support and beamtime. CHESS is supported by NSF and NIH/NIGMS under NSF award DMR-1332208, and MacCHESS is supported by NIH/NIGMS award GM-103485. This manuscript has been authored by UT-Battelle LLC under DOE Contract No. DE-AC05-00OR22725 with the U.S. Department of Energy. The publisher, by accepting the article, acknowledges that the U.S. Government retains a non-exclusive, paid-up, irrevocable, worldwide license to publish or reproduce the published form of this manuscript, or allow others to do so, for the U.S. Government purposes.

References

(1) Frost, S. C., and McKenna, R. (2013) Carbonic Anhydrase: Mechanism, Regulation, Links to Disease, and Industrial Applications. Springer Science & Business Media.

(2) Aggarwal, M., Boone, C. D., Kondeti, B., and McKenna, R. (2013) Structural annotation of human carbonic anhydrases. *J. Enzyme Inhib. Med. Chem. 28*, 267–277.

(3) Smith, K. S., Jakubzick, C., Whittam, T. S., and Ferry, J. G. (1999) Carbonic anhydrase is an ancient enzyme widespread in prokaryotes. *Proc. Natl. Acad. Sci. U. S. A. 96*, 15184–15189.

(4) Smith, K. S., and Ferry, J. G. (2000) Prokaryotic carbonic anhydrases. *FEMS Microbiol. Rev. 24*, 335–366.

(5) Fukuzawa, H., Suzuki, E., Komukai, Y., and Miyachi, S. (1992) A gene homologous to chloroplast carbonic anhydrase (icfA) is essential to photosynthetic carbon dioxide fixation by Synechococcus PCC7942. *Proc. Natl. Acad. Sci. U. S. A. 89*, 4437–4441.

(6) Guilloton, M. B., Lamblin, A. F., Kozliak, E. I., Gerami-Nejad, M., Tu, C., Silverman, D., Anderson, P. M., and Fuchs, J. A. (1993) A physiological role for cyanate-induced carbonic anhydrase in Escherichia coli. *J. Bacteriol. 175*, 1443–1451.

(7) Kusian, B., Sültemeyer, D., and Bowien, B. (2002) Carbonic anhydrase is essential for growth of Ralstonia eutropha at ambient CO(2) concentrations. *J. Bacteriol. 184*, 5018–5026.

(8) Merlin, C., Masters, M., McAteer, S., and Coulson, A. (2003) Why is carbonic anhydrase essential to Escherichia coli? *J. Bacteriol. 185*, 6415–6424.

(9) Mitsuhashi, S., Ohnishi, J., Hayashi, M., and Ikeda, M. (2004) A gene homologous to beta-type carbonic anhydrase is essential for the growth of Corynebacterium glutamicum under atmospheric conditions. *Appl. Microbiol. Biotechnol. 63*, 592–601.

(10) Burghout, P., Cron, L. E., Gradstedt, H., Quintero, B., Simonetti, E., Bijlsma, J. J. E., Bootsma, H. J., and Hermans, P. W. M. (2010) Carbonic anhydrase is essential for Streptococcus pneumoniae growth in environmental ambient air. *J. Bacteriol. 192*, 4054–4062.

(11) Valdivia, R. H., and Falkow, S. (1997) Fluorescence-based isolation of bacterial genes expressed within host cells. *Science 277*, 2007–2011.

(12) Bury-Moné, S., Mendz, G. L., Ball, G. E., Thibonnier, M., Stingl, K., Ecobichon, C., Avé, P., Huerre, M., Labigne, A., Thiberge, J.-M., and De Reuse, H. (2008) Roles of alpha and beta carbonic anhydrases of Helicobacter pylori in the urease-dependent response to acidity and in colonization of the murine gastric mucosa. *Infect. Immun. 76*, 497–509.

(13) Guilloton, M. B., Korte, J. J., Lamblin, A. F., Fuchs, J. A., and Anderson, P. M. (1992) Carbonic anhydrase in Escherichia coli. A product of the cyn operon. *J. Biol. Chem. 267*, 3731–3734.

(14) Götz, R., Gnann, A., and Zimmermann, F. K. (1999) Deletion of the carbonic anhydrase-like gene NCE103 of the yeast Saccharomyces cerevisiae causes an oxygen-sensitive growth defect. *Yeast Chichester Engl. 15*, 855–864.

(15) Clark, D., Rowlett, R. S., Coleman, J. R., and Klessig, D. F. (2004) Complementation of the yeast deletion mutant DeltaNCE103 by members of the beta class of carbonic anhydrases is dependent on carbonic anhydrase activity rather than on antioxidant activity. *Biochem. J. 379*, 609–615.

(16) Rowlett, R. S. (2010) Structure and catalytic mechanism of the beta-carbonic anhydrases. *Biochim. Biophys. Acta 1804*, 362–373.

(17) Richard, P., Le Floch, R., Chamoux, C., Pannier, M., Espaze, E., and Richet, H. (1994) Pseudomonas aeruginosa outbreak in a burn unit: role of antimicrobials in the emergence of multiply resistant strains. *J. Infect. Dis. 170*, 377–383.

(18) Kalai, S., Achour, W., Abdeladhim, A., Bejaoui, M., and Ben Hassen, A. (2005) [Pseudomonas aeruginosa isolated in immunocompromised patients: antimicrobial resistance, serotyping, and molecular typing]. *Médecine Mal. Infect. 35*, 530–535.

(19) Mesaros, N., Nordmann, P., Plésiat, P., Roussel-Delvallez, M., Van Eldere, J., Glupczynski, Y., Van Laethem, Y., Jacobs, F., Lebecque, P., Malfroot, A., Tulkens, P. M., and Van Bambeke, F. (2007) Pseudomonas aeruginosa: resistance and therapeutic options at the turn of the new millennium. *Clin. Microbiol. Infect. Off. Publ. Eur. Soc. Clin. Microbiol. Infect. Dis. 13*, 560–578.

(20) Rehm, B. H. A. (2008) Pseudomonas: Model Organism, Pathogen, Cell Factory. John Wiley & Sons.

(21) Diamond, L. W., and Akinfiev, N. N. (2003) Solubility of CO2 in water from −1.5 to 100 °C and from 0.1 to 100 MPa: evaluation of literature data and thermodynamic modelling. *Fluid Phase Equilibria 208*, 265–290.

(22) Lotlikar, S. R., Hnatusko, S., Dickenson, N. E., Choudhari, S. P., Picking, W. L., and Patrauchan, M. A. (2013) Three functional β-carbonic anhydrases in Pseudomonas aeruginosa PAO1: role in survival in ambient air. *Microbiol. Read. Engl. 159*, 1748–1759.

(23) Alterio, V., Hilvo, M., Di Fiore, A., Supuran, C. T., Pan, P., Parkkila, S., Scaloni, A., Pastorek, J., Pastorekova, S., Pedone, C., Scozzafava, A., Monti, S. M., and De Simone, G. (2009) Crystal structure of the catalytic domain of the tumor-associated human carbonic anhydrase IX. *Proc. Natl. Acad. Sci. U. S. A. 106*, 16233–16238.

(24) Aggarwal, M., Kondeti, B., Tu, C., Maupin, C. M., Silverman, D. N., and McKenna, R. (2014) Structural insight into activity enhancement and inhibition of H64A carbonic anhydrase II by imidazoles. *IUCrJ 1*, 129–135.

(25) Smith, K. S., Ingram-Smith, C., and Ferry, J. G. (2002) Roles of the conserved aspartate and arginine in the catalytic mechanism of an archaeal beta-class carbonic anhydrase. *J. Bacteriol. 184*, 4240–4245.

(26) Rowlett, R. S., Tu, C., McKay, M. M., Preiss, J. R., Loomis, R. J., Hicks, K. A., Marchione, R. J., Strong, J. A., Donovan, G. S., and Chamberlin, J. E. (2002) Kinetic characterization of wild-type and proton transfer-impaired variants of beta-carbonic anhydrase from Arabidopsis thaliana. *Arch. Biochem. Biophys. 404*, 197–209.

(27) Björkbacka, H., Johansson, I. M., and Forsman, C. (1999) Possible roles for His 208 in the active-site region of chloroplast carbonic anhydrase from Pisum sativum. *Arch. Biochem. Biophys. 361*, 17–24.

(28) Domsic, J. F., Avvaru, B. S., Kim, C. U., Gruner, S. M., Agbandje-McKenna, M., Silverman, D. N., and McKenna, R. (2008) Entrapment of carbon dioxide in the active site of carbonic anhydrase II. *J. Biol. Chem. 283*, 30766–30771.

(29) Sjöblom, B., Polentarutti, M., and Djinovic-Carugo, K. (2009) Structural study of X-ray induced activation of carbonic anhydrase. *Proc. Natl. Acad. Sci. U. S. A. 106*, 10609–10613.

(30) Kim, C. U., Wierman, J. L., Gillilan, R., Lima, E., and Gruner, S. M. (2013) A high-pressure cryocooling method for protein crystals and biological samples with reduced background X-ray scatter. *J. Appl. Crystallogr. 46*, 234–241.

(31) Kim, C. U., Kapfer, R., and Gruner, S. M. (2005) High-pressure cooling of protein crystals without cryoprotectants. *Acta Crystallogr. D Biol. Crystallogr. 61*, 881–890.

(32) Otwinowski, Z. and Minor, W. (1997) Processing of X-ray diffraction data collected in oscillation mode. *Methods in Enzymology 276,* 307-26.

(33) Pinard, M. A., Lotlikar, S. R., Boone, C. D., Vullo, D., Supuran, C. T., Patrauchan, M. A., and McKenna, R. (2015) Structure and inhibition studies of a type II beta-carbonic anhydrase psCA3 from Pseudomonas aeruginosa. *Bioorg. Med. Chem. 23(15),* 4831-8.

(34) Adams, P. D., Afonine, P. V., Bunkóczi, G., Chen, V. B., Davis, I. W., Echols, N., Headd, J. J., Hung, L.-W., Kapral, G. J., Grosse-Kunstleve, R. W., McCoy, A. J., Moriarty, N. W., Oeffner, R., Read, R. J., Richardson, D. C., Richardson, J. S., Terwilliger, T. C., and Zwart, P. H. (2010) PHENIX: a comprehensive Python-based system for macromolecular structure solution. *Acta Crystallogr. D Biol. Crystallogr. 66,* 213–221.

(35) Brünger, A. T. (1992) Free R value: a novel statistical quantity for assessing the accuracy of crystal structures. *Nature 355*, 472–475.

(36) Emsley, P., and Cowtan, K. (2004) Coot: model-building tools for molecular graphics. *Acta Crystallogr. D Biol. Crystallogr. 60,* 2126–2132.

(37) Kimber, M. S., and Pai, E. F. (2000) The active site architecture of Pisum sativum beta-carbonic anhydrase is a mirror image of that of alpha-carbonic anhydrases. *EMBO J. 19*, 1407–1418.

(38) Cronk, J. D., Rowlett, R. S., Zhang, K. Y. J., Tu, C., Endrizzi, J. A., Lee, J., Gareiss, P. C., and Preiss, J. R. (2006) Identification of a novel noncatalytic bicarbonate binding site in eubacterial beta-carbonic anhydrase. *Biochemistry (Mosc.) 45*, 4351–4361.

(39) Rowlett, R. S., Tu, C., Lee, J., Herman, A. G., Chapnick, D. A., Shah, S. H., and Gareiss, P. C. (2009) Allosteric site variants of Haemophilus influenzae beta-carbonic anhydrase. *Biochemistry (Mosc.) 48,* 6146–6156.

(40) Krissinel, E., and Henrick, K. (2007) Inference of macromolecular assemblies from crystalline state. *J. Mol. Biol. 372*, 774–797.

(41) Cronk, J. D., Endrizzi, J. A., Cronk, M. R., O'neill, J. W., and Zhang, K. Y. (2001) Crystal structure of E. coli beta-carbonic anhydrase, an enzyme with an unusual pH-dependent activity. *Protein Sci. Publ. Protein Soc. 10*, 911–922.

(42) Huang, S., Hainzl, T., Grundström, C., Forsman, C., Samuelsson, G., and Sauer-Eriksson, A. E. (2011) Structural studies of β-carbonic anhydrase from the green alga Coccomyxa: inhibitor complexes with anions and acetazolamide. *PloS One 6*, e28458.

Table 1. Crystallographic data collection and refinement statistics.

PDB ACCESSION #	5BQ1
Data Collection Statistics	
Temperature (K)	100
Wavelength (Å)	0.977
Space group	I222
Unit-cell (Å, °): *a, b, c*	71.8, 78.1, 87.7
Reflections: Theoretical, Measured	32819, 32530
Resolution (Å)	29.1 – 1.6 (1.65 – 1.60)*
[a]R_{sym}	0.08 (0.50)
I/σ(I)	72.8 (6.1)
Completeness (%)	99.3 (98.3)
Redundancy	14.1 (10.9)
Final Model Statistics	
[b]R_{cryst} (%)	17.3 (21.4)
[c]R_{free} (%)	19.9 (22.3)
[d]No. of atoms: *Protein, ligand*[e]*, water*	1675, 3 (2),103
R.M.S.D.: *Bond lengths* (Å), *angles* (°)	0.006, 0.99
Ramachandran statistics (%): *favored, allowed, outliers*	98.5, 1.5, 0.0
Average B-factors (Å^2): *Main chain, side chain, CO_2 (active site), CO_2 (interface), solvent*	29.4, 34.8, 40.6, 22.4, 35.5

*Values in parenthesis represent highest resolution bin. [a]$R_{sym} = \Sigma (|I - \langle I \rangle|)/ \Sigma \langle I \rangle$. [b]$R_{cryst} = (\Sigma |Fo| - |Fc|/ \Sigma |F_{obs}|) \times 100$. [c]$R_{free}$ is calculated in same manner as R_{cryst}, except that it uses 5% of the reflection data omitted from refinement. [d]Includes alternate conformations. [e]Value in parenthesis represent total number of ligands bound in the whole structure.

Figure Legends

Figure 1: Surface representation of (A) hCA II, and (B) psCA3. Beige and green regions represent hydrophilic and hydrophobic residues of the active site, respectively. Stick representation of active site for (C) hCA II, and (D) psCA3. The active site zinc is depicted as a magenta sphere (only one active site of psCA3 dimer is visible in this view). For all subsequent figures, residues will be as labeled, ordered waters depicted as red spheres (in this figure only the ZBS and deep water are shown), zinc as a magenta sphere, H–bonds represented by red dashes, and distances given in Å.

Figure 2: Left, cartoon representation of the functional dimeric form of psCA3. Green mesh is the difference (F_o-F_c) electron density for the two CO_2 binding sites, contoured at 2.0σ. Right, details of the CO_2 binding sites. Blue mesh, refined ($2F_o$-F_c) electron density after modeling building and refinement, contoured at 1.6σ.

Figure 3: Hydrogen bond network in psCA3 active site: (A) open (without CO_2), (B) with CO_2. Residues are as labeled. Beige and green regions represent hydrophilic and hydrophobic residues, respectively. Note the displacement of deep water on CO_2 binding.

Figure 4: Secondary binding site for another molecule of CO_2 shown at the dimeric interface as (A) cartoon, and (B) sticks (zoomed-in). The two monomers are colored yellow and cyan.

Figure 5: Cross-eyed stereo view of CO_2 in the active site of (A) hCA II, and (B) psCA3. Residues are as labeled.

Figure 6: Superposition of unbound psCA3 (grey) and CO_2-bound (green) represented as a (A) cartoon, and (B) zoomed-in sticks, showing slight perturbation in two active site residues.

Figure 1

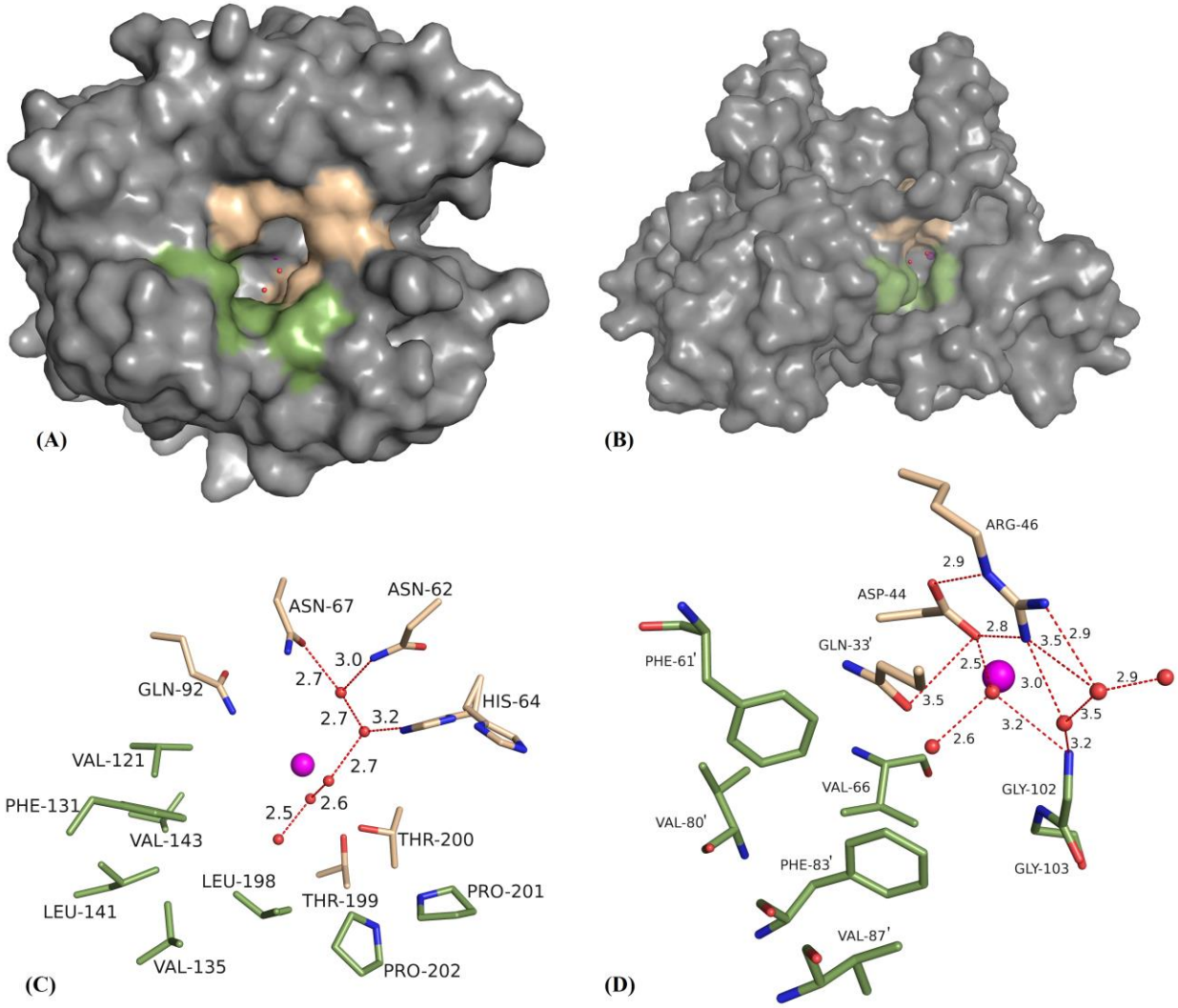
(A)
(B)
ASN-67
ASN-62
3.0
2.7
GLN-92
2.7
3.2
HIS-64
VAL-121
2.7
PHE-131
2.5
2.6
VAL-143
THR-200
LEU-198
THR-199
PRO-201
LEU-141
VAL-135
PRO-202
(C)
ARG-46
2.9
ASP-44
2.8
3.5
2.9
PHE-61'
GLN-33'
2.5
3.0
3.5
2.9
3.5
3.2
2.6
3.2
VAL-66
GLY-102
VAL-80'
PHE-83'
GLY-103
VAL-87'
(D)

Figure 2

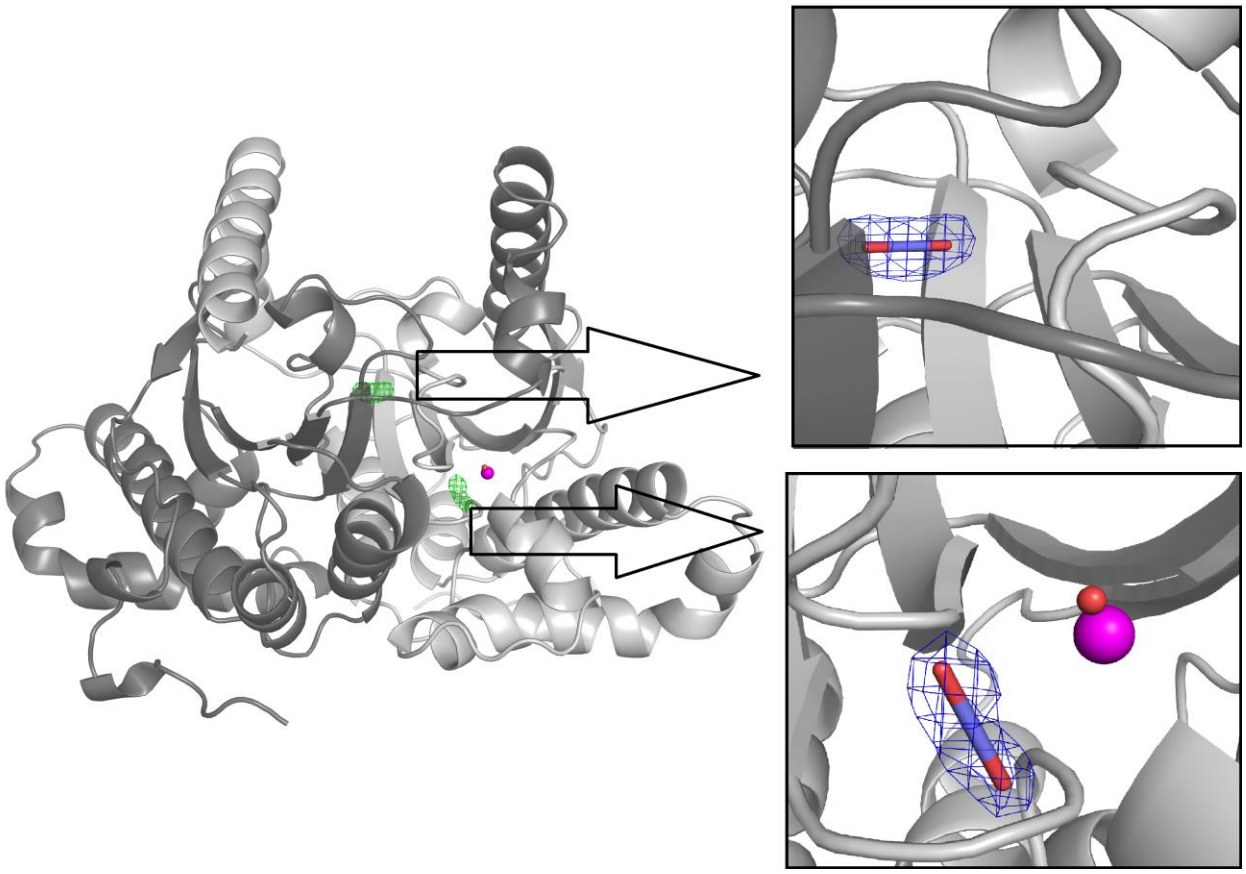

Figure 3

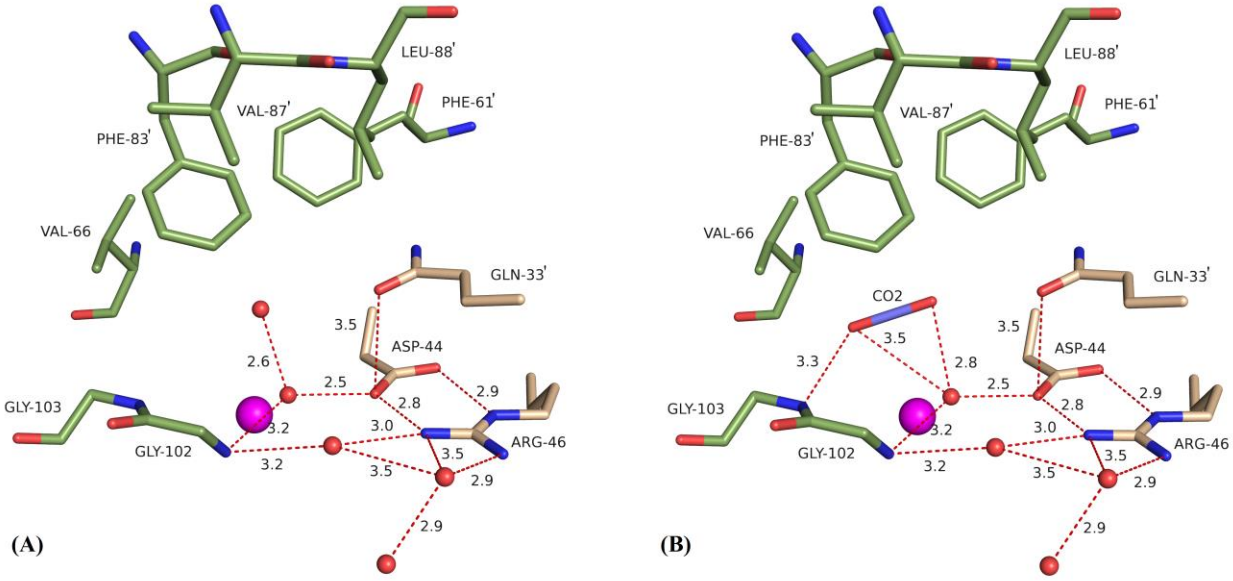
LEU-88'
VAL-87'
PHE-61'
PHE-83'
VAL-66
GLN-33'
ASP-44
GLY-103
GLY-102
ARG-46
CO2
(A)
(B)

Figure 4

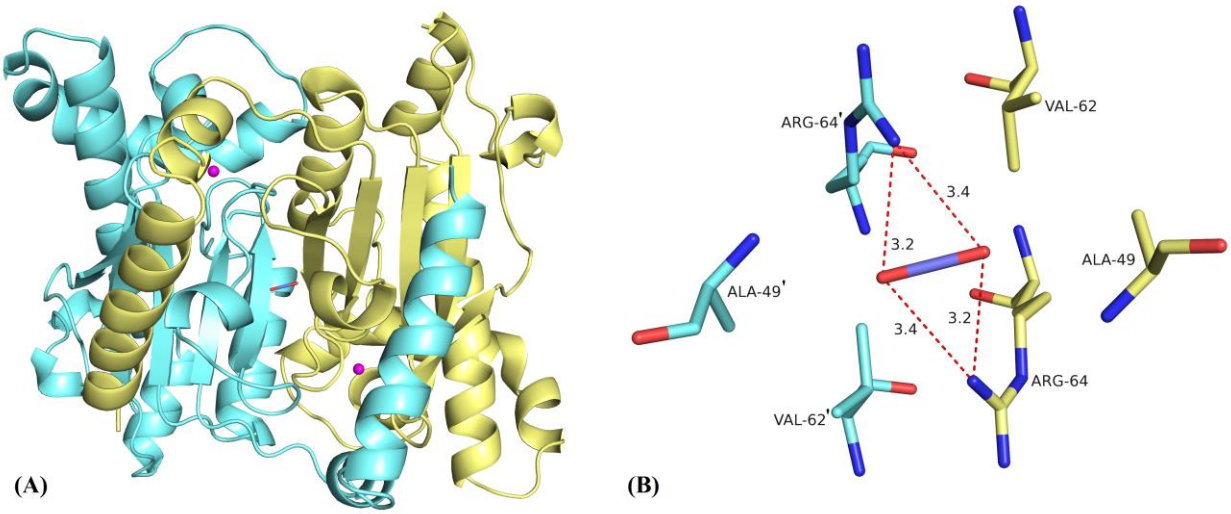

Figure 5

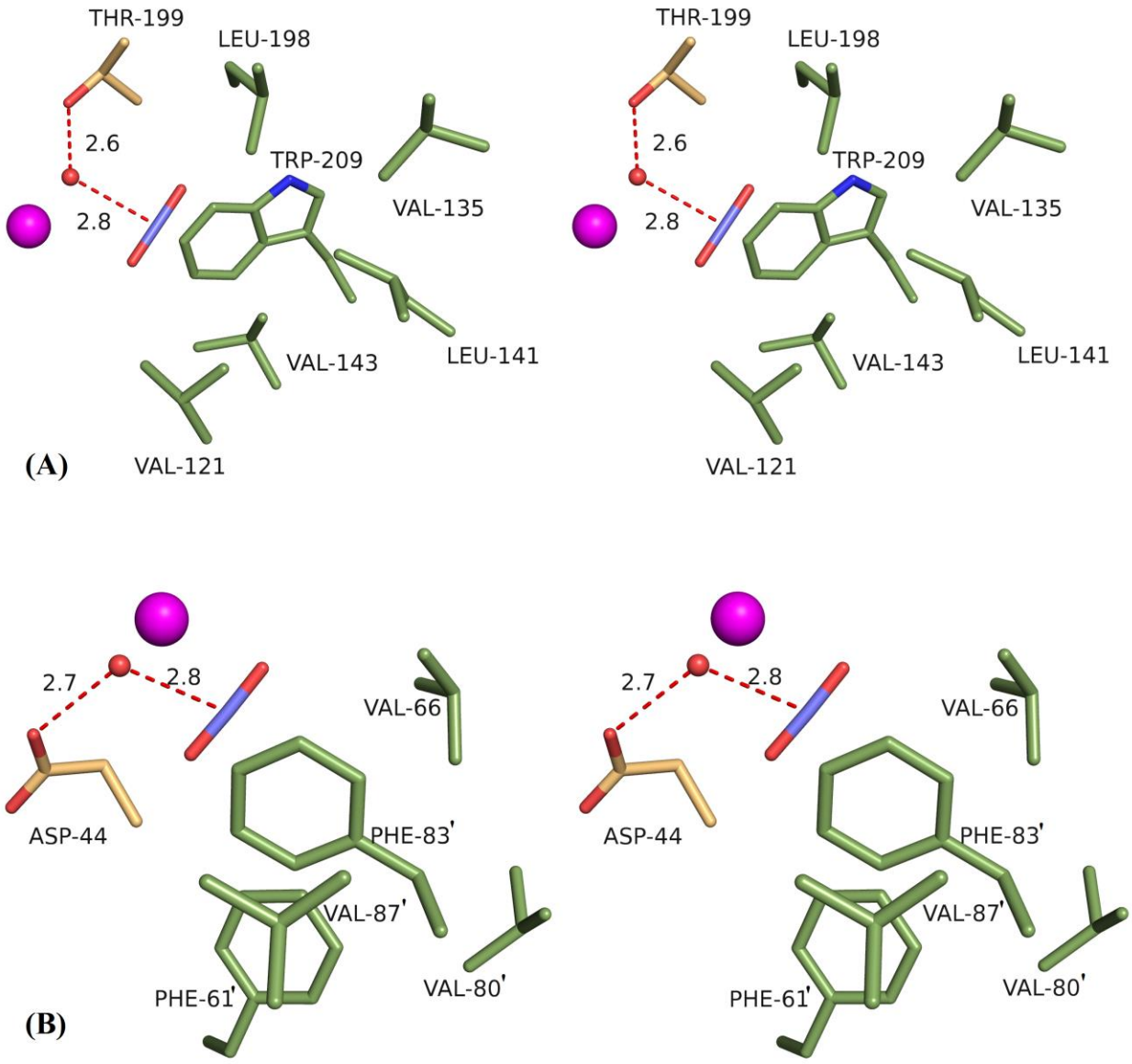
THR-199
LEU-198
2.6
TRP-209
2.8
VAL-135
VAL-143
LEU-141
VAL-121
(A)
THR-199
LEU-198
2.6
TRP-209
2.8
VAL-135
VAL-143
LEU-141
VAL-121
2.7
2.8
VAL-66
ASP-44
PHE-83'
VAL-87'
PHE-61'
VAL-80'
(B)
2.7
2.8
VAL-66
ASP-44
PHE-83'
VAL-87'
PHE-61'
VAL-80'

Figure 6

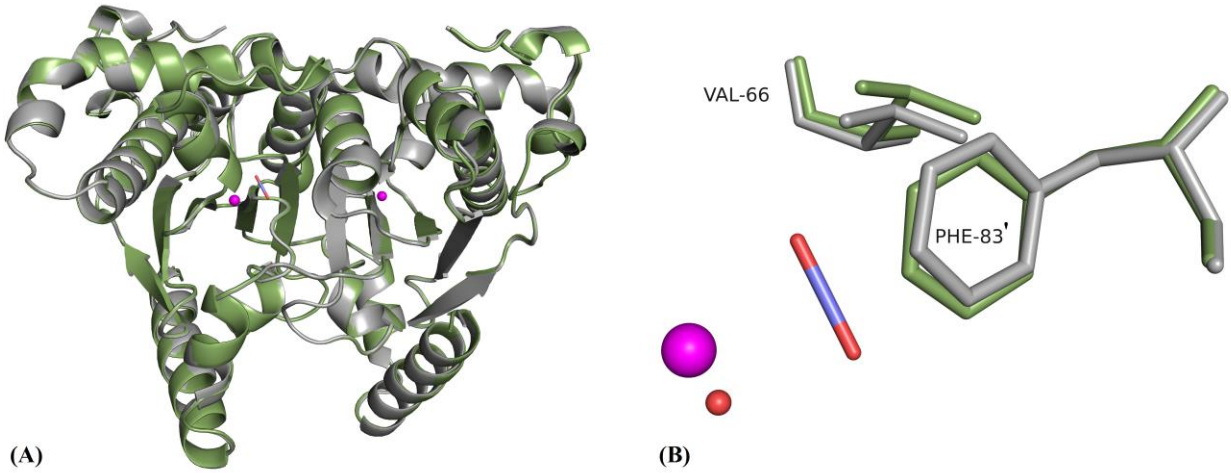

TOC Graphic

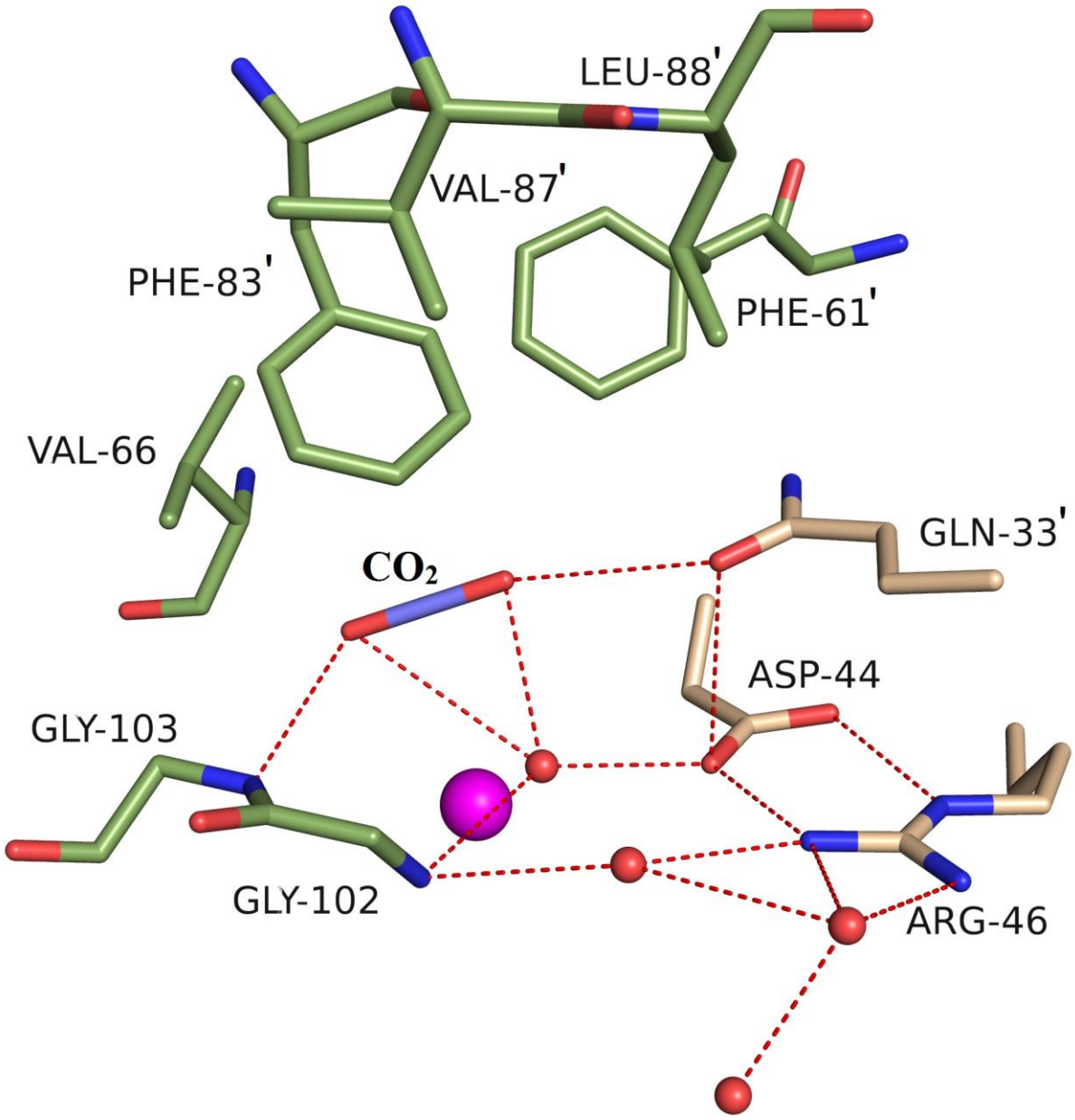
LEU-88'
VAL-87'
PHE-83'
PHE-61'
VAL-66
GLN-33'
CO2
ASP-44
GLY-103
GLY-102
ARG-46